Applied Physics Letters

Tunable band-pass optical vortex processor enabled by wash-out-refill chiral superstructures

Cite as: Appl. Phys. Lett. **118**, 151102 (2021); https://doi.org/10.1063/5.0041117
Submitted: 19 December 2020 . Accepted: 03 March 2021 . Published Online: 12 April 2021

Chun-Ting Xu, Peng Chen, Yi-Heng Zhang, Xing-Yu Fan, Yan-Qing Lu, and Wei Hu

Applied Physics Letters ARTICLE scitation.org/journal/apl

Tunable band-pass optical vortex processor enabled by wash-out-refill chiral superstructures

Cite as: Appl. Phys. Lett. **118**, 151102 (2021); doi: 10.1063/5.0041117
Submitted: 19 December 2020 · Accepted: 3 March 2021 ·
Published Online: 12 April 2021

Chun-Ting Xu, Peng Chen,[a] Yi-Heng Zhang, Xing-Yu Fan, Yan-Qing Lu, and Wei Hu[a]

AFFILIATIONS

National Laboratory of Solid State Microstructures, Key Laboratory of Intelligent Optical Sensing and Manipulation, and College of Engineering and Applied Sciences, Nanjing University, Nanjing 210093, China

[a]Authors to whom correspondence should be addressed: chenpeng@nju.edu.cn and huwei@nju.edu.cn

ABSTRACT

The manipulation of spatial parameters of light is at the cutting edge of optics. It is an interesting and important task to explore wavefront modulation approaches with a continuously tunable working band and dynamically switchable functions. Here, we program the alignment of a polymerizable cholesteric liquid crystal by a dynamic photo-patterning technique. After UV curing and a wash-out-refill process, the designed chiral superstructure is well reconstructed. By this means, a Dammann grating encoded q-plate is fabricated and its function as an optical vortex processor is demonstrated. The working band is electrically tuned and covers a broad range of 137 nm. The switching of mode conversion is achieved on a second scale for given wavelengths based on the electric-driven band shift. This strategy offers a platform for multi-dimensional dynamic control of light and may bring more possibilities to optical imaging, informatics, and micromanipulations.

Light can be depicted by different dimensions including time, frequency, and space domains, thus providing a multi-dimensional carrier of information. For instance, in optical communications, the signal is encoded via a fast switching of light sequentially in each channel. Hundreds of channels with a series of separated frequencies are multiplexed to significantly increase the bandwidth. Nowadays, multiple spatial parameters, such as amplitude, phase, and polarization,[1] are modulated to further expand the capacity of optical networks. Orbital angular momentum (OAM) is a new degree of freedom arising from the spiral phase front $\exp(im\theta)$ of an optical vortex (OV), where m is the topological charge and θ is the azimuthal angle.[2] Due to the theoretically infinite number of m, it shows great potential in high-capacity optical communications.[3,4] Besides, OVs and their arrays have attracted widespread interest in nano-fabrication, optical tweezers, super-resolution imaging, and high-dimensional quantum informatics as well.[5] Particularly, the compatibility of spatial phase manipulation with time and frequency modulations is highly desirable in OAM-integrated wavelength division multiplexing, wavelength selective optical manipulations, and hyperspectral imaging.

The photo-patterning of traditional nematic liquid crystals (LCs) enables a point-to-point way for geometric phase modulation and arbitrary wavefront control.[6,7] However, the conversion efficiency of such elements is usually sinusoidally dependent on the wavelength (except for the delicately designed multi-twist structure[8]), thus hindering the band-selective mode encoding. Cholesteric liquid crystals (CLCs), as self-assembled chiral photonic crystals, possess a spin-selective photonic bandgap (PBG).[9] Through manipulating the local orientation of the CLC helix, the geometric phase can be endowed into the reflected light within the PBG, while the reflection is highly suppressed outside the PBG.[10–12] This supplies a practical way for the spatial light modulation in a bandpass manner.[13,14] Recently, exploring dynamic PBG control has remained a hot topic in CLC-based planar optics.[10,15,16] Compared with other stimulus, electrical driving is preferred owing to its compactness, faster response, and better stability and reliability.[17,18] Unfortunately, due to the competition between dielectric and elastic torques of CLC, the helical structure will collapse under a strong electric field, thus making the electrical tunability unachievable. Polymer stabilization helps to solve this problem and enables the shift of the long-wavelength band edge.[10,19] Additionally, the switch of functions can be realized via vanishing or recovering the chiral structures by altering the applied voltages and frequencies.[20] A continuous shift of PBG is indispensable for the dynamic control of the working band.[21] For a wash-out-refill system of polymer-templated CLC, the PBG can be driven reversibly by the electric field.[22] This may offer a revolutionary platform for the multi-dimensional dynamic control of light. Therefore, it is a meaningful task to develop techniques for preprogramming the polymer-templated CLCs and systematically investigate their properties of geometric phase modulation and electrical tunability.

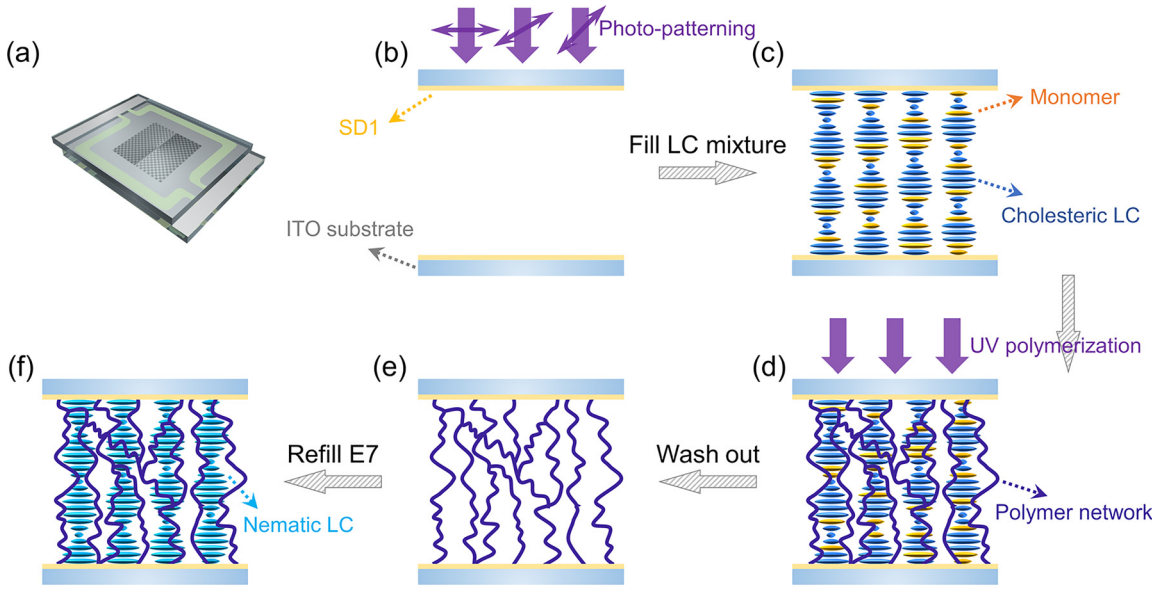

FIG. 1. Fabrication process of wash-out-refill chiral superstructures. (a) Schematic of the DQP cell. (b) Empty cell configuration and photo-patterning. (c) Filling the polymerizable LC mixture. (d) UV polymerization. (e) Polymer network after washing out. (f) Refilling LC E7.

In this work, we introduce a dynamic photo-patterning technique to program a polymer-templated CLC. The space-variant geometric phase of a Dammann grating encoded q-plate is imprinted. After a wash-out-refill process, the designed chiral superstructure is well reconstructed. Reflective polychromatic OV arrays are generated in high efficiency, and the reflection band is electrically tuned covering a broad range of 137 nm. Based on the band shift, the OAM switching for a given wavelength can be achieved on a second scale. OAM detection and transformation are carried out as well. This work provides a promising strategy for multi-dimensional dynamic control of light with soft matter-based planar optics.

Here, a tunable bandpass OV array generator, namely, Dammann-q-plate (DQP), is chosen for demonstration, which is promising in simultaneous OAM processing, parallel laser fabrication, and micromanipulation. As shown in Fig. 1(a), the DQP is a typical element exhibiting space-variant geometric phase. Its phase function is formulated as $\varphi_{\mathrm{DQP}} = m\theta + \varphi_{\mathrm{DG}}$, which is a direct integration of the phase of a q-plate[23] and that of a Dammann grating.[24] The DQP can diffract the incident light into objective orders on demand and form an OV array with equal-energy distribution. For instance, we select the normalized phase transition point to be 0.5[24] and the topological charge to be 1, and thus, four equal-intensity OV orders with $|m| = 1$ should be obtained. Meanwhile, the reflective geometric phase is twice the initial orientation angle of CLC helixes and its sign is determined by the chirality.[10–12,25] Referring to this principle, the director distribution diagram can be easily calculated through reducing by half the phase function of the designed DQP [Fig. 2(a)].

The procedure to accomplish the DQP in a wash-out-refill CLC is briefly illustrated in Fig. 1. First, a 8 μm-thick empty cell with indium-tin-oxide glass substrates spin-coated with the photoalignment agent (SD1, Dai-Nippon Ink and Chemicals, Japan) is placed at the image plane of the digital-micro-mirror-device-based microlithography system,[26] and a multi-step partly overlapping exposure process[27,28] is performed to deliver the designed distributions accordingly [Fig. 1(b)]. Second, the UV polymerizable LC is mixed by nematic LC (E7, HCCH, China), chiral dopant (R5011, HCCH, China), LC reactive monomers (HCCH, China), and photo initializer Diphenyl ketone (Shanghai Lingfeng Chemical Reagent Co. Ltd, China) at a weight ratio of 73.7: 2.1: 23.2: 1. LC reactive monomers are mixed by RM257, RM82, RM006, RM021, and RM010 at a weight ratio of 30: 15: 20: 20: 15. The LC mixture is stirred magnetically at

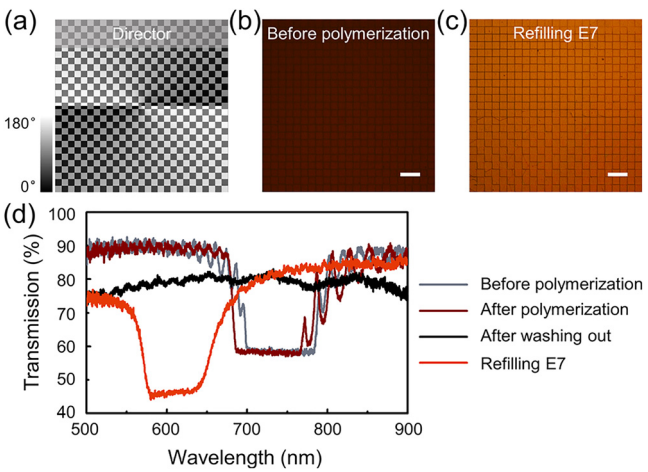

FIG. 2. (a) The director distribution diagram of the designed 2×2 DQP with $m = 1$. The color variation from black to white represents the axis varying from 0° to 180°. POM images of the DQP (b) before polymerization and (c) after refilling E7. Both scale bars indicate 100 μm. (d) Transmission spectra of the sample in four different states.

1000 rpm at 70 °C for 2 hours and then infiltrated into the cell by capillarity action [Fig. 1(c)]. After the sample cools down, it is exposed under a UV LED (M365LP1-C1, Thorlabs, USA) for 5 min for polymerization [Fig. 1(d)]. The sample is immersed in acetone for 10 h to wash out LCs and unreacted monomers and then dried at room temperature for 5 h. Accordingly, a cholesteric polymer network is left [Fig. 1(e)]. Finally, nematic LC E7 is refilled into the cell. Chiral superstructures are reconstructed [Fig. 1(f)], preserving the initial reflective geometric phase.

Figures 2(b) and 2(c) show the reflective polarization optical microscope (POM) images before polymerization and after refilling. Dark boundary lines consistent with the designed pattern [Fig. 2(a)] are clearly observed, resulting from the 90° shift of the LC director astride. The uniform reflection and color in other regions indicate ordered helical superstructures. We record the transmission spectra during the fabrication procedure as shown in Fig. 2(d). The central wavelength of PBG is $\lambda_C = (n_o + n_e)p/2$, where n_o/n_e is the ordinary/extraordinary refractive index and p is the helix pitch of CLC. After polymerization, λ_C blue shifts from 740 nm to 726 nm due to the pitch shortening caused by the volume shrinkage in cross-linking.[29] The PBG vanishes after washing out as expected, and it reappears after refilling E7 with a final λ_C value of 610 nm. The significant PBG shift is attributed to the incomplete reoccupation, which is restricted by the high viscosity of LCs and low density of the nanopore in the washing-out template.[30]

To verify the electro-optical tunability of the bandpass OV array generator, 1 kHz square-wave signals with different voltages are applied to the wash-out-refill CLC sample. As shown in Fig. 3(a), when electric field E increases from 0 V/μm to 26 V/μm, the long band edge λ_L shifts from 660 nm to 604 nm, while the short band edge λ_S shifts from 570 nm to 523 nm. It is notable that the PBG is well preserved during the whole band shift process. The central wavelength of the PBG λ_C blue shifts by 52 nm (607 nm to 555 nm). It needs to be noticed that the change in the long band edge ($\Delta\lambda_L = 56$ nm) is slightly larger that of the short band edge ($\Delta\lambda_S = 47$ nm), which means that the bandwidth reduces during blue shift. The PBG shift under the electric field is attributed to the gradual pitch contraction induced by the translation of the polymer network driven by voltages.[22] Meanwhile, thanks to the dielectric anisotropy, the nematic LCs within the polymer network tilt gradually, which leads to the decrease in n_e and the reduction in the bandwidth. As a result, a continuous color change is observed in corresponding micrographs [Fig. 3(c)].

Figure 3(b) schematically illustrates the optical setup for the OV measurements. A supercontinuum laser (SuperK EVO, NKT Photonics, Denmark) combined with a multi-channel acousto-optic tunable filter (SuperK SELECT, NKT Photonics, Denmark) is adopted to output monochromatic or multicolor lasers. Thanks to the specific band and spin selectivity of the chiral superstructures, only the circular polarization component of the light in PBG with the same handedness

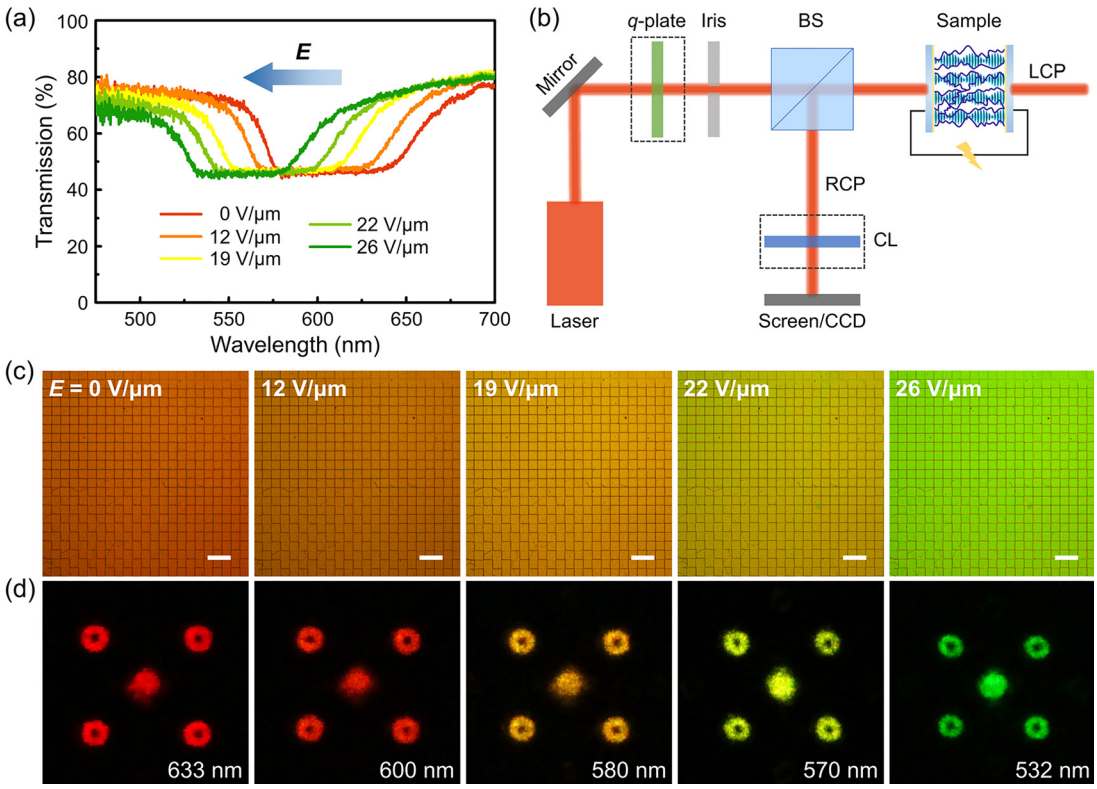

FIG. 3. Tunable bandpass OV array generator. (a) Dependency of the PBG shift on applied voltage. (b) The schematic illustration of the optical testing setup. BS, nonpolarizing beam splitter; RCP, right circular polarization; LCP, left circular polarization; CL, cylindrical lens. (c) Micrographs at different voltages. (d) Corresponding reflected diffraction patterns at different wavelengths. The applied voltages and the wavelengths of incident light are labeled. All scale bars are 100 μm.

of the CLC will be reflected and encoded with the designed geometric phase. The rest of the light propagates through the sample and experiences a wavelength-dependent phase delay.[14] Half of the reflected light is separated by the beam splitter (BS) and then projects onto the screen. As shown above, via tuning the electric field, the PBG can cover a broad range of 137 nm (523 nm to 660 nm). We select a series of separate wavelengths in the PBG of CLC for measurements. Figure 3(d) exhibits their diffraction patterns captured using a digital camera (EOS M, Canon, Japan). 2 × 2 OV arrays carrying the same topological charge are demonstrated from green to red. The diffraction efficiencies (intensity ratios of objective orders to total reflection) of individual generated OVs in Fig. 3(d) are measured. An average value of 13.58% ± 1.43% and a good energy uniformity are achieved. The obtained total efficiency (54.31% ± 2.26%) is consistent with the theoretical value (65.61%), indicating a high efficiency. It is almost independent of the wavelength in the range of 532 nm–633 nm. According to generalized Snell's law,[31] the deflection angle θ_x of output OV satisfies $\theta_x = \sin^{-1}\left(\frac{\lambda}{2\pi}\frac{d\varphi}{dx}\right)$. Its positive correlation with the incident wavelength leads to the pattern size reducing toward shorter wavelengths. This reversibility and repeatability of the tuning process will benefit practical applications.

The electric-driven band shift enables the dynamic switching of the OV array. For instance, a dual-wavelength laser (532 nm and 633 nm) is chosen to demonstrate the OV array switching. As vividly shown in Fig. 4(a), the green/red OV array turns on/off when 26 V/μm is applied. It recovers to the initial state when the field is removed. The central order is the superposition of zero order of one wavelength within the PBG and the direct reflection of the other outside the PBG, thus exhibiting a mixed color. Dynamic switching between the two states can be realized by alternately applying and removing the voltage. Figure 4(b) depicts the response properties. We define the response time as the time interval when the intensity changes between 10% and 90% and reverse. The switch on/off times for 633 nm and 532 nm are 10.2 s/1.8 s and 7.8 s/2.9 s, respectively. All of them are on a second scale.

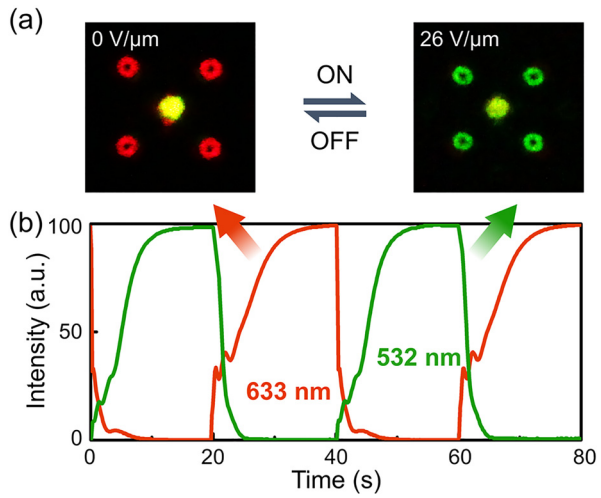

FIG. 4. Function switch based on the PBG shift. (a) Diffraction patterns of a dual-channel laser at 532 and 633 nm in voltage on/off states, respectively. (b) The responsiveness of the tunable bandpass OV array generator.

Besides OV generating, the DQP can also work as parallel OAM adders. In this case, the output topological charge m_{out} equals the sum of the topological charge of incident beam m_{in} and m. In addition, such adders can satisfy a broad wavelength range via tuning applied voltages. Here, q-plates with $m_{in} = -1$, $+1$, and -2 are inserted between the light source and the BS [Fig. 3(b)], separately. 2.5 V, 2.6 V, and 2.7 V are applied on these q-plates to satisfy the halfwave conditions of 633 nm, 570 nm, and 532 nm, respectively. POM images of q-plates and the intensity distribution of generated OVs are exhibited in Fig. 5. After being reflected by the DQP ($m = -1$), the addition operation of topological charge is performed. To characterize m_{out}, a cylindrical lens ($f = 100$ mm) is inserted in the reflective light path behind the BS, and a charge-coupled device (CCD) is put on the focal plane to record the pattern. The topological charge can be recognized by the number and the tilt direction of dark stripes.[32] The measured m_{out} values are −2, 0, and −3, respectively. In the special case of $m_{in} = -m$, all diffraction orders turn to Gaussian beams as shown in Fig. 5(b), which can be adopted for the OAM detection.

Here, we encode the geometric phase to a wash-out-refill CLC through a dynamic photo-patterning technique. Using this method, spatial phase modulation of light is efficiently achieved. The electrically tuned PBG enables a selectivity in the frequency domain. Based on the band shift, fast switching of functions is demonstrated for a given wavelength. This strategy is ready for multi-dimensional dynamic control of light. To further extend the tunable wavelength range, temperature control can be introduced. The PBG remains stable from 20 °C to 55 °C without voltage applied and blue shifts to 530 nm via further increasing the temperature. By the combination of electric and temperature control, the PBG would cover the whole visible range. Besides DQP, various phase elements with interesting functions can be

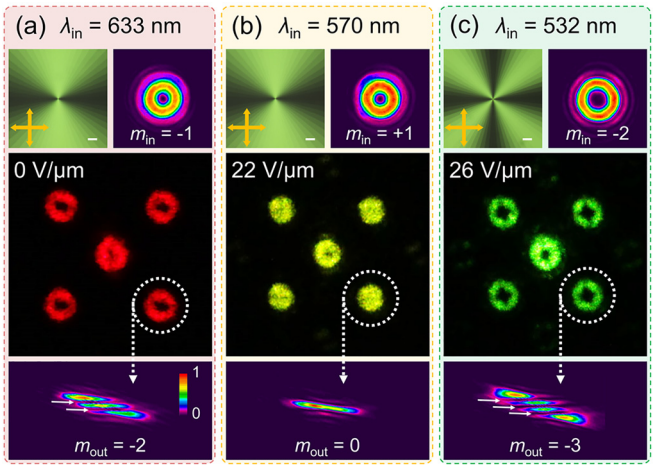

FIG. 5. OAM transformation and detection. Up left images show POM micrographs of q-plates with different topological charges: (a) $m = -1$, (b) $m = +1$, and (c) $m = -2$. Up right images reveal the intensity of OVs generated by the q-plates correspondingly. Middle images show reflective diffraction patterns of OVs after the DQP at different applied voltages and wavelengths: (a) 0 V/μm and 633 nm, (b) 22 V/μm and 570 nm, and (c) 26 V/μm and 532 nm. Bottom images show the topological charge detection results of the OVs marked by white circles. The directions of polarizers and analyzers are indicated by double-ended arrows. All scale bars are 100 μm. The color bar indicates the relative optical intensity.

reasonably expected via presetting alignment patterns. For example, Dammann vortex gratings can be designed for the free control of diffraction lattices and topological charges of OVs.[33] Additionally, owing to the bandpass and spin-dependent reflection of the CLC chiral superstructures, different light modulations can be encoded to different wavelengths and spins by stacking a series of especially designed elements. Besides, spontaneous LC topological defects are promising for the OV generation. In particular, the *in situ* OV generation induced by the photo-sensitive walls[34] supplies an efficient solution to eliminate the alignment of the optical setup, and vortex lattices can emerge simultaneously in single LC cell under a low-frequency oscillatory electric field.[35]

In conclusion, we accomplish reflective geometric phase encoding in a wash-out-refill CLC using a dynamic photo-patterning technique. A Dammann grating encoded *q*-plate is generated for demonstration. Its function as a tunable bandpass optical vortex processor including an OV array generator and parallel OAM adder is verified. The electric-driven band shift covers a broad range from 523 nm to 660 nm, and second-scale mode switching is achieved. This work provides a reliable, low-cost, and easy-fabrication strategy for tunable bandpass planar optics and will inspire more fantastic applications, such as hyperspectral imaging, high capacity communication, and heterogeneous microfabrication.

This work was supported by the National Natural Science Foundation of China (NSFC) (Nos. 62035008, 61922038, and 12004175), the Natural Science Foundation of Jiangsu Province (No. BK20200311), the Fundamental Research Funds for the Central Universities (No. 021314380185), and the Innovation and Entrepreneurship Program of Jiangsu Province. The authors gratefully thank Rui Yuan and Yuan Liu for their kind assistants on using facilities.

DATA AVAILABILITY

The data that support the findings of this study are available from the corresponding author upon reasonable request.

REFERENCES

[1]A. Forbes, A. Dudley, and M. Mclaren, Adv. Opt. Photonics **8**, 200–227 (2016).
[2]L. Allen, M. W. Beijersbergen, R. J. Spreeuw, and J. P. Woerdman, Phys. Rev. A **45**, 8185–8189 (1992).
[3]A. E. Willner, H. Huang, Y. Yan, Y. Ren, N. Ahmed, G. Xie, C. Bao, L. Li, Y. Cao, Z. Zhao, J. Wang, M. P. J. Lavery, M. Tur, S. Ramachandran, A. F. Molisch, N. Ashrafi, and S. Ashrafi, Adv. Opt. Photonics **7**, 66–106 (2015).
[4]J. Wang, Photonics Res. **4**, B14–B28 (2016).
[5]Y. Shen, X. Wang, Z. Xie, C. Min, X. Fu, Q. Liu, M. Gong, and X. Yuan, Light Sci. Appl. **8**, 90 (2019).
[6]J. Kim, Y. Li, M. N. Miskiewicz, C. Oh, M. W. Kudenov, and M. J. Escuti, Optica **2**, 958–964 (2015).
[7]P. Chen, B. Y. Wei, W. Hu, and Y. Q. Lu, Adv. Mater. **32**, 1903665 (2020).
[8]K. J. Hornburg, R. K. Komanduri, and M. J. Escuti, J. Opt. Soc. Am. B **36**, D28–D33 (2019).
[9]I. C. Khoo and S. T. Wu, *Optics and Nonlinear Optics of Liquid Crystals* (World Scientific, Singapore, 1993).
[10]J. Kobashi, H. Yoshida, and M. Ozaki, Nat. Photonics **10**, 389–392 (2016).
[11]M. Rafayelyan, G. Tkachenko, and E. Brasselet, Phys. Rev. Lett. **116**, 253902 (2016).
[12]R. Barboza, U. Bortolozzo, M. G. Clerc, and S. Residori, Phys. Rev. Lett. **117**, 053903 (2016).
[13]J. Kobashi, H. Yoshida, and M. Ozaki, Phys. Rev. Lett. **116**, 253903 (2016).
[14]P. Chen, L. L. Ma, W. Duan, J. Chen, S. J. Ge, Z. H. Zhu, M. J. Tang, R. Xu, W. Gao, T. Li, W. Hu, and Y. Q. Lu, Adv. Mater. **30**, 1705865 (2018).
[15]K. Yin, Y. H. Lee, Z. He, and S. T. Wu, Opt. Express **27**, 5814–5823 (2019).
[16]P. Chen, L. L. Ma, W. Hu, Z. X. Shen, H. K. Bisoyi, S. B. Wu, S. J. Ge, Q. Li, and Y. Q. Lu, Nat. Commun. **10**, 2518 (2019).
[17]Z. G. Zheng, Y. Q. Lu, and Q. Li, Adv. Mater. **32**, 1905318 (2020).
[18]P. C. Wu, G. W. Wu, I. V. Timofeev, V. Y. Zyryanov, and W. Lee, Photonics Res. **6**, 1094–1100 (2018).
[19]Y. Inoue, H. Yoshida, H. Kubo, and M. Ozaki, Adv. Opt. Mater. **1**, 256–263 (2013).
[20]R. Chen, Y. H. Lee, T. Zhan, K. Yin, Z. W. An, and S. T. Wu, Adv. Opt. Mater. **7**, 1900101 (2019).
[21]B. A. Kowalski, V. P. Tondiglia, K. M. Lee, D. R. Evans, T. J. White, and M. S. Mills, Opt. Express **27**, 16571–16577 (2019).
[22]S. M. Wood, J. A. J. Fells, S. J. Elston, and S. M. Morris, Macromolecules **49**, 8643–8652 (2016).
[23]L. Marrucci, C. Manzo, and D. Paparo, Phys. Rev. Lett. **96**, 163905 (2006).
[24]C. Zhou and L. Liu, Appl. Opt. **34**, 5961–5969 (1995).
[25]M. Rafayelyan and E. Brasselet, Phys. Rev. Lett. **120**, 213903 (2018).
[26]P. Chen, B. Y. Wei, W. Ji, S. J. Ge, W. Hu, F. Xu, V. Chigrinov, and Y. Q. Lu, Photonics Res. **3**, 133–139 (2015).
[27]P. Chen, W. Ji, B. Y. Wei, W. Hu, V. Chigrinov, and Y. Q. Lu, Appl. Phys. Lett. **107**, 241102 (2015).
[28]Y. H. Zhang, P. Chen, S. J. Ge, T. Wei, J. Tang, W. Hu, and Y. Q. Lu, Appl. Phys. Lett. **117**, 081101 (2020).
[29]J. B. Guo, H. Cao, J. Wei, D. W. Zhang, F. Liu, G. H. Pan, D. Y. Zhao, W. L. He, and H. Yang, Appl. Phys. Lett. **93**, 201901 (2008).
[30]J. D. Lin, C. L. Chu, H. Y. Lin, B. You, C. T. Horng, S. Y. Huang, T. S. Mo, C. Y. Huang, and C. R. Lee, Opt. Mater. Express **5**, 1419–1430 (2015).
[31]N. Yu, P. Genevet, M. A. Kats, F. Aieta, J. P. Tetienne, F. Capasso, and Z. Gaburro, Science **334**, 333–337 (2011).
[32]V. Denisenko, V. Shvedov, A. S. Desyatnikov, D. N. Neshev, W. Krolikowski, A. Volyar, M. Soskin, and Y. S. Kivshar, Opt. Express **17**, 23374–23379 (2009).
[33]T. Lei, M. Zhang, Y. Li, P. Jia, G. N. Liu, X. G. Xu, Z. H. Li, C. J. Min, J. Lin, C. Y. Yu, H. B. Niu, and X. C. Yuan, Light Sci. Appl. **4**, e257 (2015).
[34]R. Barboza, U. Bortolozzo, G. Assanto, E. Vidal-Henriquez, M. G. Clerc, and S. Residori, Phys. Rev. Lett. **109**, 143901 (2012).
[35]M. G. Clerc, M. Kowalczyk, and V. Zambra, Sci. Rep. **10**, 19324 (2020).